

## Nusselt-number scaling and azimuthal velocity profiles in a rotating cylindrical tank with a radial horizontal convection imposed to model atmospheric polar vortices

Wisam K. Hussam<sup>1,2</sup>, Martin P. King,<sup>3</sup> Luca Montabone<sup>4</sup> and Gregory J. Sheard<sup>1</sup>

<sup>1</sup>Department of Mechanical and Aerospace Engineering, Monash University, Adelaide, VIC 3800, Australia

<sup>2</sup>Electromechanical Department, University of Technology, Baghdad, Iraq

<sup>3</sup>Bjerknes Centre for Climate Research, Uni Research, NO 5007, Bergen, Norway

<sup>4</sup>Atmospheric, Oceanic and Planetary Physics, University of Oxford, Parks Road, Oxford OX13PU, United Kingdom

### Abstract

A system idealizing the polar atmosphere is constructed featuring a rotating cylindrical container with radial fluid flux driven by a linear radial temperature profile along the base. This system is investigated numerically using a spectral-element solver employing a Boussinesq approximation to model buoyancy. The study focuses on the scaling of mean Nusselt number with Rayleigh number over a range of Reynolds numbers characterizing the tank rotation rate.

It is found that for  $Ra \lesssim 10^4$ , Nusselt number is independent of Reynolds number and the flow is dominated by diffusion. At intermediate Rayleigh numbers, mixed convection is observed with Nusselt number decreasing with increasing Reynolds number. Beyond  $Ra \approx 10^6$  convective flow begins to dominate, first at low Reynolds numbers, with higher Reynolds number data progressively collapsing onto a universal power-law trend that is independent of Reynolds number. This trend is found to follow theoretical and observed scalings for horizontal convection in rectangular enclosures, i.e.  $Nu \propto Ra^{1/5}$ .

### Introduction

The convection of a fluid contained between two parallel plates and heated from below (Rayleigh–Bénard convection, RBC) has received much attention over the years because of its importance in understanding the flow dynamics and thermally driven turbulence [14, 13, 8]. The key parameter characterizing RBC is Rayleigh number, which quantifies the strength of thermal forcing on the flow.

Horizontal convection defines flows that are driven by temperature differentials imposed along a horizontal boundary [6]. This is in contrast to RBC in which the temperature differential is in the vertical direction. The effect of rotation on convection flows is important in many industrial applications as well as in astrophysical and geophysical flows, including meridional overturning circulation in the ocean [9], Earth's core [4], and solar and mantle convections [5, 10]. The motivation for the present paper is the stability of atmospheric polar vortices; particularly towards understanding the striking geometric patterns adopted by polar vortices across various planets [3], and to better understand the sudden configuration changes that on Earth affect weather at latitudes impacting on Australia.

Laboratory fluid models have proved useful for the study of polar vortex instability (e.g. [1]), though these models have typically featured mechanical forcing mechanisms dissimilar to atmospheric mechanisms. In the present paper, cylinder rotation mimics Earth's rotation, and radial horizontal convection drives an annular radial flux circulating outward near the base and returning poleward at the top surface. Conservation of angular momentum accelerates the angular velocity of poleward-

moving fluid, spinning it into a vortex in an analogous manner to the generation of atmospheric polar vortices in the polar convection cell.

As a first approximation of the atmospheric system, this model disregards gamma-plane effects associated with the change in the Coriolis effect with latitude in the vicinity of the pole [1]. Moreover, while the controlling parameters for this system are Reynolds and Rayleigh number, the parameters of interest when considering swirling atmospheric flows are typically the Rossby number (relating inertial to Coriolis forces) and the Ekman number (relating viscous to Coriolis forces). The Ekman number is related to the reciprocal of the Reynolds number, but the Rossby number, which relates the angular velocity of the model polar vortex to the background rotation, is flow-dependent. A goal of the present study is to understand the effects of Reynolds number and Rayleigh number on this flow, and how the Rossby number varies with these parameters.

To consider the suitability of this model for implementation in a laboratory setting, a wide range of Rayleigh number ( $3.2 \leq Ra \leq 10^{10}$ ) and Reynolds number ( $3.2 \leq Re \leq 10^3$ ) are considered in this study.

### Numerical model and methodology

The system comprises an open rotating cylindrical tank, filled with fluid, and with a radial temperature distribution applied at the base. The tank radius  $R$  and height  $H$  combine to define an aspect ratio  $AR = H/R$ , which in this study is fixed at  $AR = 0.4$ . The system is depicted in figure 1.

Given an angular velocity of the cylinder,  $\Omega$ , the azimuthal velocity imposed on the impermeable base and side wall is  $u_\theta = r\Omega$ , where  $r$  is the radial coordinate. To model a free surface, a stress-free condition is imposed on the top boundary ( $u_z = 0, \partial u_r / \partial z = \partial u_\theta / \partial z = 0$ ). The side wall is thermally insulated by imposition of a zero normal temperature gradient, and to simplify the computational model, no heat loss is permitted through the stress-free top surface, which is also approximated as being thermally insulated. A linear temperature profile increasing by  $\delta T$  from  $r = 0$  to  $r = R$  is imposed along the base to drive the horizontal convection in the  $z$ - $r$  plane

A Boussinesq approximation for fluid buoyancy is employed, in which density differences in the fluid are neglected except through the gravity term in the momentum equation. Under this approximation the energy equation reduces to a scalar advection-diffusion equation for temperature which is evolved in conjunction with the velocity field. The fluid temperature is related linearly to the density via a thermal expansion coefficient  $\alpha$ .

The dimensionless Navier–Stokes equations governing a

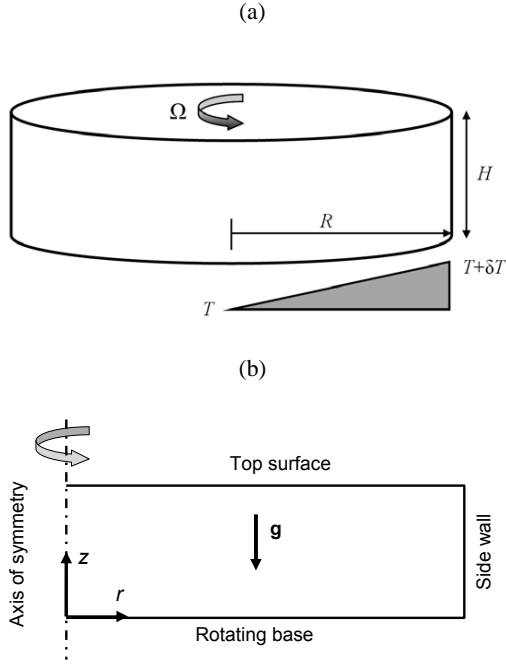


Figure 1: (a) A schematic diagram of the system under investigation, with temperature difference  $\delta T$  varying radially along the base, and (b) the meridional semi-plane of the cylindrical tank on which computations are performed.

Boussinesq fluid may be written as

$$\frac{\partial \mathbf{u}}{\partial t} = -(\mathbf{u} \cdot \nabla) \mathbf{u} - \nabla p + \frac{1}{Re} \nabla^2 \mathbf{u} + \hat{\mathbf{g}} T \frac{Ra}{Re^2 Pr}, \quad (1)$$

$$\nabla \cdot \mathbf{u} = 0, \quad (2)$$

$$\frac{\partial T}{\partial t} = -(\mathbf{u} \cdot \nabla) T + \frac{1}{Pr Re} \nabla^2 T, \quad (3)$$

where  $\mathbf{u}$ ,  $p$ ,  $t$ ,  $Re$ ,  $Ra$ ,  $Pr$ ,  $\hat{\mathbf{g}}$  and  $T$  are the velocity vector, kinematic static pressure, time, Reynolds number, Rayleigh number, Prandtl number, a unit vector in the direction of gravity, and temperature, respectively. Here lengths, velocities, time and temperature are scaled by  $R$ ,  $R\omega$ ,  $\omega^{-1}$ ,  $\delta T$ , respectively. The Reynolds number, Rayleigh number, Prandtl number and Nusselt number are respectively defined as

$$Re = \frac{R^2 \Omega}{\nu}, \quad (4)$$

$$Ra = \frac{g \alpha \delta T R^3}{\nu k_T}, \quad (5)$$

$$Pr = \frac{\nu}{k_T}, \quad (6)$$

$$Nu = \frac{\overline{\partial T}}{\partial z}, \quad (7)$$

where  $g$  is the gravitational acceleration,  $\nu$  is the kinematic viscosity and  $k_T$  is the thermal diffusivity of the fluid. The mean Nusselt number is calculated in the present configuration by computing the average temperature gradient normal to the bottom wall. Throughout this study  $Pr = 6.14$ , which approximates water at laboratory conditions.

The governing flow equations (1)-(3) are computed on a two-dimensional axisymmetric domain using a high-order in-house

solver, which employs a spectral element method for spatial discretization and a third-order time integration scheme based on backwards-differencing. The solver has been validated and employed widely (e.g. Refs. [12, 13, 7]).

A rectangular mesh comprising 1560 was constructed to discretize the meridional ( $r$ - $z$ ) semi-plane. Care was taken to ensure that the flow was resolved in the vicinity of the walls, and particularly the heated boundary, with coarser mesh spacing in the interior. A grid independence study determined that integrated Nusselt numbers were independent of resolution to better than 0.1% with an element polynomial degree of 5, which is used hereafter.

## Results and discussion

Nusselt number variation with Rayleigh number for different Reynolds numbers is plotted on a log-log plot in Fig. 2(a). The plot shows that at  $Ra \lesssim 10^4$ , the Nusselt number is independent of Reynolds number (the diffusion dominated regime). As  $Ra$  is increased, the Nusselt-number curves converge onto a single trend, which is nearly linear on the log-log plot, demonstrating a power-law dependence between  $Nu$  and  $Ra$ . The gradient is very close to  $1/5$ , which is in agreement with theory and observation for horizontal convection in a rectangular enclosure [11, 6, 13]. The scaling in the convection-dominated regime is further illustrated by the plot of the gradients of the trends in Fig. 2(b).

Figs. 3 and 4 plot the temperature and relative azimuthal velocity for  $Re = 10$  and  $1000$ , respectively, at different Rayleigh numbers. It can be noted that for small  $Re$ , the flow passes from a diffusion-dominated regime to a convection dominated regime prior to  $Ra \approx 10^6$ . On the other hand, for  $Re = 1000$ , the flow remains in the diffusion-dominated regime until  $Ra \approx 10^6$ , and approaches the convection-dominated regime beyond  $Ra = 10^9$ .

It can be noted from Fig. 2 that at intermediate Rayleigh numbers (between the diffusion- and convection-dominated regimes, Nusselt number decreases with increasing Reynolds number, which is consistent with the numerical finding of [14]. To further investigate the  $Nu - Re$  relationship, the effect of Reynolds number on Nusselt number at different Rayleigh number is presented in Fig. 5. The figure demonstrates that Nusselt number is independent of Reynolds number for  $Ra \lesssim 10^4$ , and at higher Rayleigh numbers, the Nusselt numbers are Reynolds-number independent until progressively higher Reynolds numbers.

A Rossby number may be defined as the ratio of the relative angular velocity of the polar vortex ( $\omega$ ) to the background rotation ( $\Omega$ ). An approximation based on the peak relative azimuthal velocity ( $u'_{\theta, \text{peak}}$ ) and its radial location ( $r_{\text{peak}}$ ) is  $\omega = u'_{\theta, \text{peak}}/r_{\text{peak}}$ . This yields a Rossby number definition

$$Ro = \frac{\omega}{\Omega} = \frac{u'_{\theta, \text{peak}}/r_{\text{peak}}}{\Omega}. \quad (8)$$

Relative azimuthal velocity profiles are plotted in Fig. 6, for various Rayleigh numbers and  $Re = 10$  and  $1000$ . The general trend is for the relative velocity to remain unaffected until Rayleigh numbers beyond the diffusion-dominated regime, whereby further Rayleigh number increases lead to an increase in peak relative azimuthal velocity. Coupled with this is a shift in the radial location of the peak from  $r = R/2$  to slightly lower radial distances. At  $Re = 1000$ , the peak relative azimuthal velocity increases to a lesser extent than at  $Re = 10$ , by almost a factor of 2. Using the definition outlined here, at  $Re = 10$

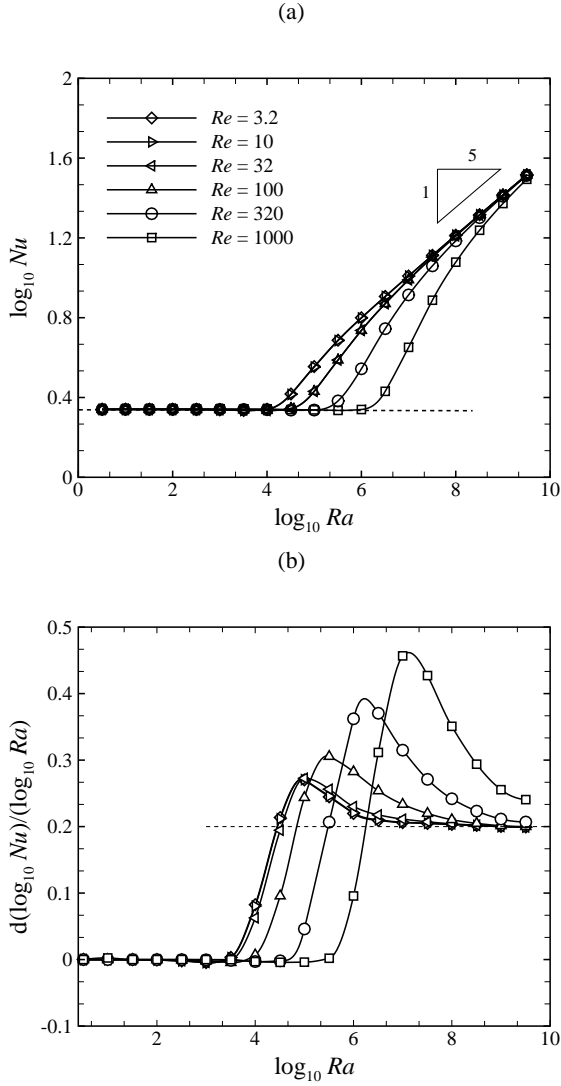


Figure 2: (a) A plot of  $\log_{10} Nu$  against  $\log_{10} Ra$  for different Reynolds number as indicated. Akima splines are fitted to the data for guidance. A dotted line shows the asymptotic  $\log_{10} Nu$ . (b) A plot of gradient of the curves in (a), calculated using finite difference. A dotted line illustrates the theoretical gradient of  $1/5$ .

the Rossby number increases from  $Ro = 0$  to  $2.1$  for  $Ra = 10^3$  to  $10^9$ , while at  $Re = 1000$  the Rossby number increases from  $Ro = 0$  to  $1.0$  for  $Ra = 10^5$  to  $10^9$ . These results suggest that this system may be useful for the study of polar vortex instability, as polar vortices manifest at Rossby numbers  $Ro < 1$  [1].

### Conclusions

Numerical simulations have considered the axisymmetric flow in an open cylindrical tank under constant rotation, and subjected to a thermal horizontal convection forcing invoking a radial poleward flux near the free surface. The results demonstrate at low Rayleigh numbers ( $Ra \lesssim 10^4$ ), the flow is diffusion-dominated with Nusselt number independent of Reynolds number and producing a zero Rossby number. At higher Rayleigh numbers (upwards of  $Ra \approx 10^6$ ) a convection-dominated regime is reached, whereby  $Nu \sim Ra^{1/5}$ . Beyond the diffusion-dominated regime, higher Rayleigh numbers produce progressively higher Rossby numbers. At  $Ra = 10^9$ ,  $Ro = 2.1$  and  $1.0$  at  $Re = 10$  and  $1000$ , respectively, which encompasses the Rossby

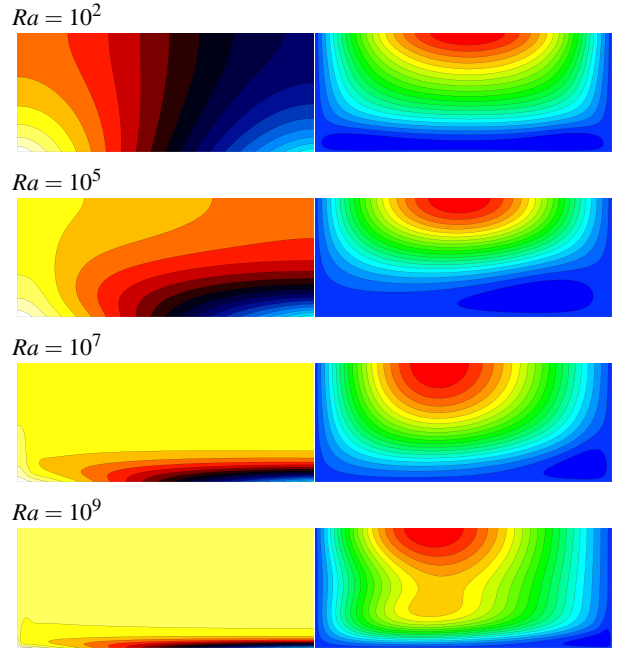


Figure 3: Contour plots of temperature (left) and azimuthal velocity relative to the tank rotation ( $u_\theta - r\Omega$ , right) at  $Re = 10$  and Rayleigh numbers as indicated, plotted on a meridional cross-section through the centre of the tank (so that the frames meet at the symmetry axis). Thermal forcing is imposed along the bottom of each of these frames. Cold to hot temperatures are denoted by contours ranging from blue through black through red to yellow. Low to high relative velocities are denoted by contours ranging from blue through to red.

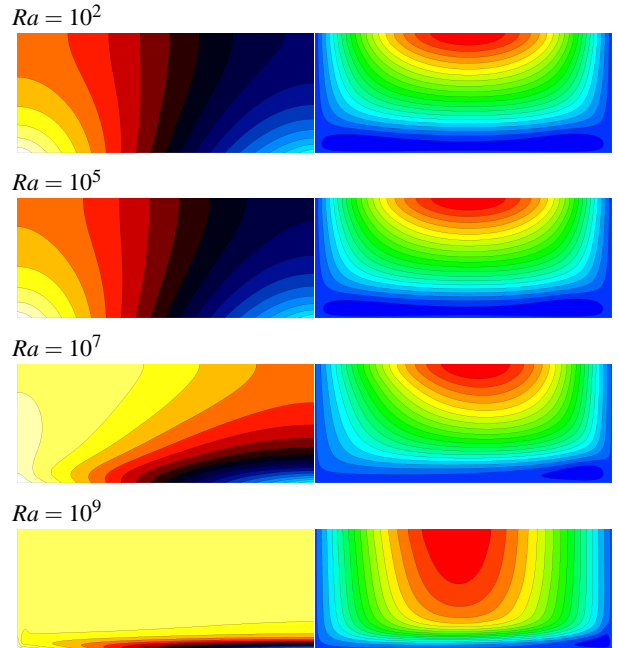


Figure 4: Contour plots of temperature (left) and azimuthal velocity relative to the tank rotation ( $u_\theta - r\Omega$ , right) at  $Re = 1000$  and Rayleigh numbers as indicated. Orientation and shading are as per Fig. 3.

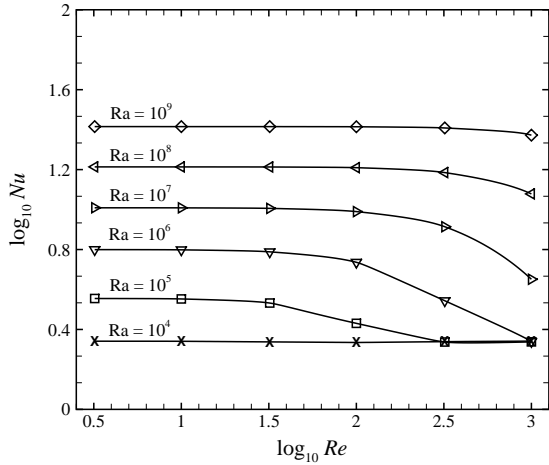
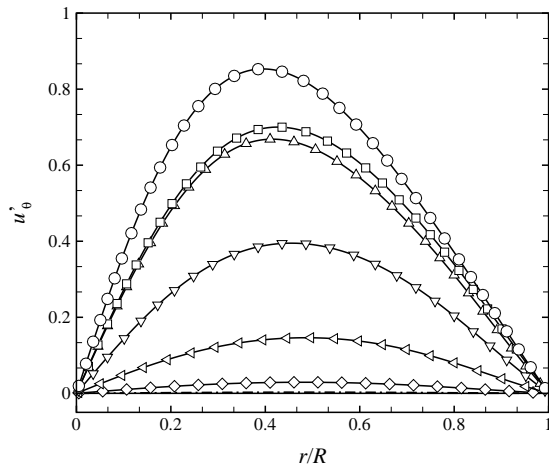


Figure 5: A plot of  $\log_{10} Nu$  against  $\log_{10} Re$  for different Rayleigh numbers as indicated.

(a)



(b)

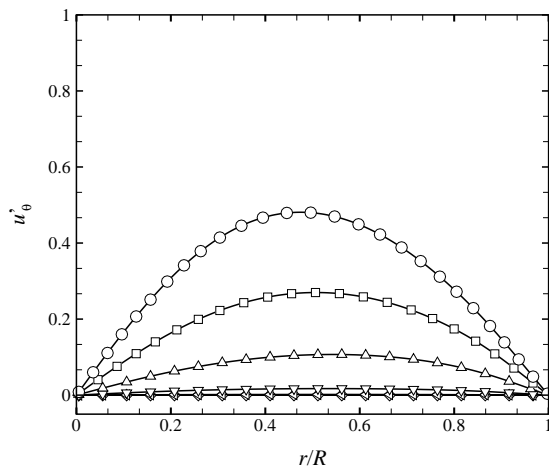


Figure 6: The relative azimuthal velocity along the free surface for different Rayleigh numbers at (a)  $Re = 10$  and (b)  $Re = 1000$ .

number range relevant for polar vortex flows.

### Acknowledgements

This work is supported by the Australian Research Council through Discovery Grant DP120100153, by the National Computational Infrastructure (NCI) Merit Allocation Scheme, and by Monash University through a Faculty of Engineering Seed Grant.

### References

- [1] Aguiar, A.C.B., Read, P.L., Wordsworth, R.D., Salter, T. and Yamazaki, Y.H., A Laboratory Model of Saturn's North Polar Hexagon, *Icarus*, **206**, 2010, 755–763.
- [2] Akima, H., A New Method of Interpolation and Smooth Curve Fitting Based on Local Procedures, *J. Assoc. Comput. Mach.*, **17** (4), 1970, 589–602.
- [3] Fletcher, L.N., Irwin, P.G.J., Orton, G.S., Teanby, N.A., Achterberg, R.K., Bjoraker, G.L., Read, P.L., Simon-Miller, A.A., Howett, C., de Kok, R., Bowles, N., Calcutt, S.B., Hesman, B. and Flasar, F.M., Temperature and Composition of Saturn's Polar Hot Spots and Hexagon, *Science*, **319**, 2008, 79–81.
- [4] Glatzmaier, G.A., Coe, R.S., Hongre, L. and Roberts, P.H., The role of the Earth's mantle in controlling the frequency of geomagnetic reversals, *Nature*, **401**, 1999, 885–890.
- [5] Glatzmaier, G.A., Coe, R.S., Hongre, L. and Roberts, P.H., Convection driven zonal flows and vortices in the major planets, *Chaos*, **4**, 1994, 123–134.
- [6] Hughes, G.O. and Griffiths, R.W., Horizontal Convection, *Annu. Rev. Fluid Mech.*, **40**, 2008, 185–208.
- [7] Hussam, W.K., Thompson, M.C. and Gregory J. Sheard, Dynamics and Heat Transfer in a Quasi-Two-Dimensional MHD Flow Past a Circular Cylinder in a Duct at High Hartmann Number, *Int. J. Heat Mass Trans.*, **54**, 2011, 1091–1100.
- [8] King, E.M., Stellmach, S. and Aurnou, J.M., Heat transfer by rapidly rotating Rayleigh-Bénard Convection, *J. Fluid Mech.*, **691**, 2012, 568–582.
- [9] Marshall, J. and Schott, F., Open-ocean convection: Observations, theory, and models, *Rev. Geophys.*, **691**, 1999, 1–64.
- [10] Miesch, M.S., The coupling of solar convection and rotation, *Solar Physics*, **192**, 2000, 59–89.
- [11] Mullarney, J.C., Griffiths, R.W. and Hughes, G.O., Convection driven by differential heating at a horizontal boundary, *J. Fluid Mech.*, **516**, 2004, 181–209.
- [12] Sheard, G.J., Leweke, T., Thompson, M.C. and Hourigan, K., Flow around an impulsively arrested circular cylinder, *Phys. Fluids*, **19**, 2007, 083601.
- [13] Sheard, G.J. and King, M.P., The influence of height ratio on Rayleigh-number scaling and stability of horizontal convection, *Appl. Math. Model.*, **35**, 2011, 1647–1655.
- [14] Zhong, J.-Q., Stevens, R.J.A.M., Clercx, H.J.H., Verzicco, R., Lohse, D. and Ahlers, G., Prandtl-, Rayleigh-, and Rossby-Number Dependence of Heat Transport in Turbulent Rotating Rayleigh-Bénard Convection, *Phys. Rev. Lett.*, **102**, 2009, 44502.